HHS Public Access

Author manuscript

Nat Methods. Author manuscript; available in PMC 2021 March 14.

Published in final edited form as:

Nat Methods. 2020 October ; 17(10): 1025–1032. doi:10.1038/s41592-020-0934-5.

In vivo detection of antigen-specific CD8 T cells by immuno-positron emission tomography

AW Woodham[1,2,*], **SH Zeigler**[3,*], **L Zeyang**[4,*], **SC Kolifrath**[1,2], **RW Cheloha**[1,2], **M Rashidian**[1,2], **R Chaparro**[5], **RD Seidel**[5], **SJ Garforth**[3], **JL Dearling**[6], **M Mesyngier**[1,4], **PK Duddempudi**[3], **AB Packard**[7], **SC Almo**[8], **HL Ploegh**[1,2]

[1]Program in Cellular and Molecular Medicine, Boston Children's Hospital, Boston, MA

[2]Department of Pediatrics, Harvard Medical School, Boston, MA

[3]Department of Biochemistry, Albert Einstein College of Medicine, Bronx, NY

[4]Department of Biology, Massachusetts Institute of Technology, Cambridge, MA

[5]Cue Biopharma, Cambridge, MA

[6]Division of Nuclear Medicine, Department of Radiology, Children's Hospital Boston

[7]Nuclear Medicine and Molecular Imaging, Boston Children's Hospital/Harvard Medical School

[8]Department of Biochemistry, Albert Einstein College of Medicine, Bronx, NY

Abstract

The immune system's ability to recognize peptides on major histocompatibility molecules (pMHCs) contributes to eradication of cancers and pathogens. Tracking these responses *in vivo* could help evaluate the efficacy of immune interventions and improve mechanistic understanding of immune responses. We employ synTacs, dimeric pMHC scaffolds of defined composition, which enable clonal-selective delivery of a variety of signaling, recruitment, and imaging modalities. We show that synTacs, when labeled with positron-emitting isotopes, can non-invasively image antigen-specific CD8 T cells *in vivo*. We imaged human papillomavirus (HPV16) E7-specific CD8 T cells by positron emission tomography with an HPV16 E7 peptide-loaded synTac in HPV16-positive tumors, following administration of a therapeutic vaccine. We also imaged influenza A virus (IAV) nucleoprotein-specific CD8 T cells in the lungs of IAV-infected mice, using an isotopically labeled flu-specific synTac. It is thus possible to visualize antigen-specific CD8 T cell populations *in vivo*, which may serve prognostic and diagnostic roles.

*Authors contributed equally

Competing interests

The authors declare no competing interest.

Introduction

Immuno-positron emission tomography (immunoPET) can monitor immune responses in living animals. Conventional antibodies (Abs) and their fragments[1] such as anti-CD8 diabodies,[2] or camelid-derived heavy chain-only Abs (VHHs), including anti-CD8 VHHs,[1,3] can serve as imaging agents for immune cell markers. These agents can track the *in vivo* distribution of bulk populations of CD8 T cells[1] and assess immune responses irrespective of antigen specificity, which yields incomplete information on immune status.[4] Activated T cells can be imaged using PET by markers such as OX40, granzyme B, or interferon γ (IFNγ).[5–7] Genetically engineered T cells can be visualized by PET by relying on conversion of labeled nucleotides.[8] However, neither surrogate markers nor genetically engineered T cells can detect antigen-specific T cells *in vivo*, as these approaches do not exploit the specificity of the T cell receptors (TCRs). Non-invasive imaging approaches that distinguish these T cells from bulk lymphocyte populations are lacking.

The TCR interacts with a major histocompatibility complex (MHC)-encoded product and its bound peptide ligand (pMHC).[9] Antigen-specific CD8 T cells are components of the adaptive immune system that kill target cells through the interaction of their TCRs with pMHCs. In some cervical cancers, these peptides are human papillomavirus (HPV)-encoded protein fragments, presented on MHC I molecules.[10] For a given pMHC, the response is typically polyclonal. T cells that recognize the pMHC use a diverse set of TCRs, composed of unique α and β subunits.[11] The affinity of a TCR for its cognate pMHC is considerably weaker than that of an antigen-specific B cell receptor (equilibrium dissociation constants of ~μM versus ñM, respectively).[12] The introduction of pMHC multimers, which compensate for affinity through increased avidity, has enabled the detection of antigen-specific T cells *ex vivo*.[13–15]

We introduce an Fc-based covalent pMHC dimer, referred to as a synTac (synapse for T cell activation) to enable selective delivery of different cargoes, including immunomodulatory molecules and imaging agents, to T cell clones of defined specificity. Because of the covalent nature of the pMHC module, the peptide is stable and non-exchangeable. Changing the encoded peptide is straightforward to enable detection of different T cell specificities. SynTacs avoid the use of foreign proteins and their associated immunogenicity, as is the case for streptavidin-based MHC tetramers.

We describe synTacs as PET imaging agents to detect antigen-specific T cells in live mice. We examined two viral models and the dominant epitopes recognized in a CD8 T cell response against them: HPV type 16 (HPV16)-induced cancer and influenza A virus (IAV) infection. Using isotopically labeled pMHC dimers, CD8 T cells that recognize these epitopes can be distinguished from bystander CD8 T cells attracted adventitiously by chemotactic cues, but which lack disease-related specificity. Any strategy aimed at eliciting cytotoxic T cells would benefit from the ability to gauge directly the presence of antigen-specific CD8 T cells at the desired location.

Results

Design of class I pMHC dimer-based PET imaging agents

SynTacs exploit covalent pMHC dimers displayed on the Fc region of murine IgG2a possessing well-characterized mutations (L235, E318A, K320A, and K322A) to reduce interactions with Fc gamma receptors and complement proteins.[16,17] Each of the C_H2 domains of the Fc region carries an N-terminal H-2D^b MHC class I molecule (heavy chain), with its peptide covalently linked to β2-microglobulin (light chain). An engineered disulfide directs association between β2m and the heavy chain (Figure 1A, Supplemental Figure 1). In HPV16-transformed cells, the immunodominant peptide recognized by CD8 T cells is RAHYNIVTF, derived from the E7 protein, and its presentation restricted by H-2D^b.[18] For IAV-infected cells, the immunodominant peptide is ASNENMETM from the nucleoprotein (NP) restricted by H-2D^b.[19] As a specificity control, we used a synTac prepared with the H-2D^b-restricted epitope (KAVYNFATM; P14) from lymphocytic choriomeningitis virus (LCMV).[20] We modified the Fc region with a C-terminal sortase recognition motif (LPETG) to enable site-specific installation of $(Gly)_3$-Lys-biotin or $(Gly)_3$-radiometal chelators (Figure 1B).[21] The MW of the synTac, as determined by size exclusion chromatography-multiple angle light scattering (SEC-MALS), is 163 ± 2.61 kDa, similar to conventional Abs (148.9 ± 3.87 kDa) (Supplemental Figure 2) and considerably smaller than pMHC tetramers (~ 270 kDa).

The functionality of the sortase motif was verified with $(Gly)_3$Lys-biotin (Figure 1C). Comparison by SDS-PAGE of the biotinylated product with a mono-biotinylated standard showed a labeling efficiency of ~80% (Supplemental Figure 3). We then installed the $(Gly)_3$-metal chelators 1,4,7-triazacyclononane-N,N',N"-triacetic acid (NOTA) and desferrioxamine (DFO) for labeling with $^{64}Cu^{2+}$ and $^{89}Zr^{4+}$, respectively.[22] We likewise used sortase to install a *trans*-cyclooctene (TCO)-functionalized peptide, followed by a 'click' reaction with a tetrazine-labeled-^{18}F-2-deoxyfluoroglucose (FDG) produced by oxime ligation.[23] Free label was removed by size-exclusion chromatography. Labeled synTacs were stable in mouse serum (Supplemental Figure 4). The injected dose (50–100 μCi (1850–3700 kBq) based on the radioisotope, corresponding to ~25 μg of synTac) was based on our experience with VHH-based imaging.[3] The amount of radioactivity at the time of imaging was ~10 μCi (370 kBq)/mouse. We were thus able to compare the performance of PET tracers using three different radioisotopes: ^{18}F, ^{64}Cu, and ^{89}Zr.

SynTacs bind to antigen-specific CD8 T cells with appropriate peptide specificity *in vitro*

Prior to *in vivo* application, we performed IFNγ enzyme-linked immunospot (ELISpot) assays to assess the specificity of synTacs *in vitro*. Mice were immunized with the HPV E7 peptide conjugated to an anti-CD11b VHH (VHH_{CD11b}-E7), in the presence of adjuvant (polyIC and anti-CD40 Ab)[22], or were infected with IAV to elicit antigen-specific CD8 T cell expansion. Splenocytes were then incubated with either the HPV E7 or IAV NP peptide, or with equimolar amounts of the corresponding synTacs. Activated antigen-specific CD8 T cells from spleens of VHH_{CD11b}-E7 treated mice secreted IFNγ in response to both HPV E7 peptide and to the HPV E7 synTac, but not to the IAV NP peptide or the IAV NP synTac (Figure 2). Similarly, CD8 T cells from IAV-infected mice secreted IFNγ only in response to

the IAV NP peptide or its corresponding synTac. Interactions between synTacs and TCRs are thus specific to the covalently-linked peptide.

Detection of CD8 T cells in HPV16 E7-expressing tumors by VHH-based immunoPET

Cancers induced by HPV16, the most common high-risk oncogenic HPV strain, express viral antigens distinct from self,[24] with the E6 and E7 genes as the primary drivers of oncogenesis.[25] Mouse models of HPV16 E7-positive tumors (e.g., C3.43 cells) mostly lack E7-specific CD8 T cells ('cold' tumors) unless the mouse is treated with immunostimulatory agents that contain or encode $E7_{49–57}$ (RAHYNIVTF).[26,27] In the presence of adjuvant, a VHH-E7 adduct that targets $CD11b^+$ cells (VHH_{CD11b}-E7) induces a stronger E7-specific T cell response than E7 peptide alone.[22] We verified by ELISpot that E7-specific T cells are present in the spleens and in C3.43 tumors of VHH_{CD11b}-E7-treated mice (Figure 3A–B). While ELISpot detects E7-specific T cells *in vitro*, it does not allow detection of these cells *in vivo*.

ImmunoPET using an anti-CD8 ^{89}Zr-labeled VHH detected bulk CD8 T cells in C3.43 tumors of VHH_{CD11b}-E7-treated mice (Figure 3C) as a reference for the experiments involving synTacs. Mice inoculated with the C3.43 tumor cell line and treated with VHH_{CD11b}-E7 together with adjuvant or with adjuvant alone were imaged eight days later. The PET images show infiltration of CD8 T cells into the E7-positive tumors in VHH_{CD11b}-E7 treated mice, unlike tumors in the adjuvant only group. While these images show an influx of CD8 T cells, only a portion may recognize the E7 epitope, the remainder being CD8 T cells of unrelated specificity. Therefore, having established their specificity *in vitro*, we next used synTacs labeled with PET radioisotopes to see whether we could image populations of antigen-specific T cells in C3.43-tumor bearing mice.

Detection of HPV16 E7-specific CD8 T cells in E7-expressing tumors by synTac-based immunoPET

Mice were inoculated with C3.43 cells. When tumors became palpable, mice were given VHH_{CD11b}-E7 and adjuvant or adjuvant alone (Supplemental Figure 5). Seven days later, mice were given the HPV E7 synTac labeled with $^{64}Cu^{2+}$ and imaged the following day. The choice of $^{64}Cu^{2+}$ was based on ease of its installation in comparison with ^{18}F or ^{89}Zr, and for compatibility with the circulatory half-life of synTacs, which is <15 minutes (Supplemental Figure 6), presumably due to rapid sequestration by the liver (see below). The PET signal observed with the ^{64}Cu-labeled HPV E7 synTac in tumors of VHH_{CD11b}-E7-treated mice was significantly stronger than that of the adjuvant-only group (Figure 4A–B, Figure 4D, and %ID/g values in Supplemental Table 1). Mice received only a single dose of VHH_{CD11b}-E7, which accounts for some variability in the response and consequently in the presence of CD8 T cells in the tumor (Figure 4D). When we imaged C3.43 tumor-bearing mice that received VHH_{CD11b}-E7 treatment with a non-cognate synTac carrying the H-$2D^b$-restricted LCMV P14 epitope, we saw no intratumoral PET signal (Figure 4C). Separately we inoculated mice with C3.43 cells on one flank and with B16 melanoma cells −which lack HPV E7− on the contralateral flank to create a setting where two tumors in the same animal differ in the antigens presented. Mice were treated with VHH_{CD11b}-E7 and adjuvant or adjuvant only and imaged with the ^{64}Cu-labeled E7 synTac. PET intensity was significantly

greater in the C3.43 tumors of VHH_{CD11b}-E7 -treated mice than in the B16 tumors in the same animal (%ID 1.25 vs 1.80; p = 0.04) (Figure 4E–F). The ratio of the PET signal observed in the C3.43 tumors to that in the B16 tumors was also significantly greater in mice treated with VHH_{CD11b}-E7 than that of controls, though it remains unclear why there was a decrease in the observed B16 signal (Figure 4G, %ID/g values in Supplemental Table 2). The signal in both tumors is similar in control mice, but is significantly increased in the C3.43 tumors following treatment known to induce HPV-specific T cells. Differences in vasculature, perfusion, pressure, and tumor size may influence synTac uptake in the two tumors.

We did not see significant accumulation of HPV E7 synTac in the spleens of VHH_{CD11b}-E7-treated mice, notwithstanding positive ELISpot results. This may reflect sensitivity of the imaging agents, because mice transgenic for a TCR that recognizes the LCMV P14 epitope showed a clear signal for the LCMV P14 synTac in the spleen (Supplemental Figure 7). The ELISpot data from Figure 3B show an average of ~250 antigen-specific T cells per 10^4 tumor cells (~2.5% of total cells) in VHH_{CD11b}-E7-treated mice, which were detectable by PET (Figure 4B), indicating the PET detection limit may be below this level. We obtained similar numbers from the lungs of IAV-infected mice, as discussed below. While these experiments clearly demonstrated the intratumoral detection of HPV16 E7-specific CD8 T cells by immunoPET, there was also accumulation of PET signal in the liver.

Detection of IAV NP-specific CD8 T cells in the lungs of IAV-infected mice by synTac-based immunoPET

We explored imaging IAV-infected mice with the IAV NP synTac (H2-D^b dimer loaded with $NP_{366–374}$ ASNENMETM). IAV-specific CD8 T cells help remove infected lung cells.[28] Using the ^{89}Zr-labeled anti-CD8 VHH, we observed strong PET signals in the lungs of IAV-infected mice nine days post infection (p.i.) (Supplemental Figure 8). We confirmed the presence of IAV NP-specific CD8 T cells in the spleens and lungs of infected mice by ELISpot (Figure 5A–B). Only the lungs of IAV-infected mice yielded a strong PET signal with the IAV NP synTac (Figure 5C–E, %ID/g values provided in Supplemental Table 3). When we imaged IAV-infected mice with the HPV E7 synTac as a specificity control, we observed no signal in lungs or spleen. Although we had no difficulty detecting the PET signal in the lungs of IAV-infected mice, the IAV NP synTac also showed strong liver accumulation. We therefore re-imaged mice that received the ^{64}Cu-labeled IAV NP synTac 9 days p.i. following euthanasia and abdominal organ resection (liver, intestines, etc.) to eliminate the observed off-target background signal from images. For quantitation after organ resection, we reset the remaining radioactivity in the mouse as the new ‘injected dose’. The ^{64}Cu-labeled IAV NP synTac PET signal in the lungs of IAV-infected mice was prominent (Figure 5G) with high %ID/g values (Figure 5F). Thus, there was ~40% of the remaining injected dose in the lungs of the IAV-infected mice imaged with the IAV synTac after removing the high background organs (i.e. liver). IAV-infected mice imaged with the HPV E7 synTac or uninfected mice imaged with the IAV NP synTac showed little or no signal (Figures 5H–5I, %ID/g values in Supplemental Table 4). All synTac immunoPET images showed strong liver signal (Supplemental Table 5, Figures 4A–4C, and Figures 5G–

I). Such uptake was observed regardless of antigen specificity, the presence of a tumor, or infection with IAV, as explored below.

C-terminal modifications do not affect non-specific organ uptake of SynTacs

Non-specific uptake of PET imaging agents complicates analyses.[21,29] Affixing polyethylene glycol (PEG) can reduce non-specific retention of VHH-based imaging agents in organs of elimination (kidneys and bladder).[3] We synthesized and attached a bifunctional substrate (Gly_3-NOTA-azide) to the C-terminus of the HPV E7 synTac, followed by installation of 20 kDa PEG using an azide-DBCO click reaction. The extent of modification was >90% (Figure 6A). This product was then labeled with $^{64}Cu^{2+}$ and used to image C3.43 tumor-bearing mice, eight days after treatment with VHH_{CD11b}-E7 (Figure 6B). PEGylation did not affect the ability of synTacs to detect E7-specific CD8 T cells in C3.43 tumors, but failed to reduce liver retention (Figure 6B). We next asked whether the radioisotope or chelator contributed to non-specific liver uptake. Regardless of the radioisotope or labeling method used, liver retention of the synTacs remained high (Figure 6C; Supplemental Table 6). Thus, differences in radiometals and their chelators or the use of ^{18}F do not explain liver retention of synTacs.

Neither glycosylation status nor FcRn engagement account for non-specific organ uptake of synTacs

Hepatocytes carry the asialoglycoprotein receptor (ASGPR) that recognizes terminal galactose residues.[30,31] Therefore, we examined the effect of Fc glycosylation on liver uptake. Prior to $^{64}Cu^{2+}$ labeling, IAV NP synTacs were treated with peptide:N-glycosidase F (PNGase F), which removed N-linked glycans, as determined by SDS-PAGE (Figure 6D). IAV-infected mice were then imaged with deglycosylated or control synTacs. Deglycosylated synTacs detected IAV NP-specific CD8 T cells in the lungs of IAV-infected mice (Figure 6E, left) with similar PET intensity to that of the glycosylated synTac (Figure 5D–E), while liver retention remained prominent. Prior injection with a large intravenous dose of asialofetuin, administered as an ASGPR competitor, failed to reduce liver uptake (Supplemental Figure 9). Interaction with FcRn on hepatocytes[32] was also ruled out, as we saw no appreciable differences in liver uptake of the IAV NP synTac between FcRn knock-out and control mice (Figure 6F, Supplemental Table 6). Thus, neither glycosylation nor FcRn interaction appears to account for liver retention of the synTacs. This also suggests that due to lack of FcRn interaction, synTacs did not engage in hepatic lysosomal recycling back into the circulation.[33] Further work is required to understand the mechanism(s) of liver retention.

Discussion

The diversity of the TCR repertoire endows the immune system with the ability to recognize antigens expressed by cancers and pathogens in the form of antigen-derived peptides presented on MHC molecules. pMHC multimers are valuable tools for TCR identification, characterization, and T cell isolation,[14] but are applied to T cells *ex vivo*.[4] The relatively large size of commonly used pMHC oligomers may complicate their use for *in vivo*

imaging. Efficient tissue penetration and relatively short circulatory half-life are essential to achieve acceptable signal to noise ratios, which are impacted by probe size.

A compelling reason for non-invasive imaging is the ability to track biological responses throughout the course of a treatment such as vaccination or immunotherapy. While blood provides access to circulating cells, the analysis of bone marrow, thymus, and secondary lymphoid organs requires more invasive methods or –in preclinical models– even euthanasia. Non-invasively tracking lymphocyte distributions in live mice over time therefore requires a different approach. ImmunoPET techniques that use antibodies or derivatives targeting surface markers on immune cells begin to address this.[1,3,29,33,34] Various PET imaging agents can monitor the *in vivo* distribution of T cell populations as well as detect intratumoral CD8 T cells,[2,3,35,36] but they do not identify antigen-specific T cells. Tools that identify antigen-specific T cells *in vivo* without the need for transfer of marked or genetically modified T cells would be highly desirable. We show that synTacs derivatized with PET isotopes can be used to track antigen-specific CD8 T cells *in vivo*.

SynTacs are built on an Fc backbone, onto which two covalent pMHC molecules are grafted, yielding constructs similar in size and organization to conventional antibodies (Supplemental Figure 2). However, synTacs are composed of building blocks in configurations that do not occur naturally, which may affect pharmacokinetic behavior. Indeed, one possible consequence could be loss of FcRn interactions, as antibodies with identical Fc segments, but different antigen-binding arms (Fabs), can differ in their interactions with FcRn.[37] Thus, the presence of two pMHCs in place of the Fab and CH1 domain could alter FcRn interaction and reduce FcRn-mediated lysosomal recycling, resulting in the observed liver uptake. Neither covalent modification nor deglycosylation of the synTacs altered non-specific liver uptake. Other modifications, such as chemical dimerization, may reduce liver retention. Notwithstanding this limitation, we could readily record antigen-specific PET signals. The size of mice imposes constraints on the distances that separate target tissues. In clinical studies these distances may be greater, allowing even better discrimination of features of interest.

We combined the spatial resolution of PET with the selective targeting of synTacs to non-invasively visualize antigen-specific T cells *in vivo* in a cancer and acute infection model. These techniques could be used in the future to correlate antigen-specific CD8 T cell localization with clinical responses, and synTacs may be valuable diagnostic and prognostic reagents. Indeed, a recent report demonstrated that the same synTac scaffold used to image the HPV E7-specific T cells could selectively deliver covalently linked IL-2 (termed ImmunoSTAT) and expand E7-specific CD8 T cells, with antitumor efficacy in the HPV-driven TC-1 tumor model.[38] These capabilities will be expanded for imaging of CD4 T cells by generating synTacs containing class II pMHCs in the future.

Online Methods

All procedures were performed in accordance with institutional guidelines and approved by the Boston Children’s Hospital Institutional Animal Care and Use Committee (IACUC protocol number 16–12-3328).

Mice, cell culture, and recombinant protein production

Specific pathogen-free female 6–8-week-old C57BL/6 mice and FcRn knock-out (KO) were purchased from Jackson Laboratory (000664 and 003982, respectively). Tumor challenge studies were performed with the C3.43 HPV16-transformed[18] and B16 melanoma murine cell lines. C3.43 cells were a gift from W Martin Kast, PhD (University of Southern California) and were maintained in Iscove's modified Dulbecco's medium (IMDM) supplemented with 10% heat-inactivated fetal bovine serum (IFS), 50 μM 2-mercaptoethanol, and 100 U/mL penicillin/streptomycin (PS). B16 cells were obtained from ATCC and maintained in Dulbecco's Modified Eagle's Medium (DMEM) supplemented with 10% IFS, and 100 U/mL PS. Cells used for tumor inoculation were propagated no longer than 2 weeks from original seed stocks. All cell lines were found to be mouse pathogen free (and *Mycoplasma pulmonis* free) by IDEXX BioResearch pathogen testing. Heptamutant sortase A from *Staphylococcus aureus* was expressed with a 6X His-tag and purified following published procedures.[39] Recombinant camelid-derived single-chain antibody fragments (VHHs) containing a C-terminal sortase A recognition motif and His-Tag (LPETG-HHHHHH) were produced following published procedures.[22] HPV E7 and IAV NP peptides were synthesized as described.[39]

SynTac design

All synTac plasmids for both heavy (MHCI α1, α2, α3 and Fc CH2, CH3) and light chains (B2M and peptide antigens; i.e., HPV E7, IAV NP, or LCMV P14) were cloned into the pcDNA3.3 vector using in-fusion cloning approaches following the manufacturer's instructions (Takara). Both chains are expressed with the B2M signal peptide to facilitate secretion from cells during protein production. The heavy chain (MHC-Fc) contains a C-terminal sortase recognition motif followed by a 6X His-tag (LPETG-HHHHHH) for post-translational modifications and purification, respectively. The heavy and light chains of the synTac construct are covalently connected using an engineered internal disulfide bond created by the A236C and R12C mutations on MHC H-2D^b and B2M, respectively. These mutations were picked as target internal disulfide mutants based on structural analysis of the MHC H-2D^b-B2M complex, and we have confirmed they hold the heavy and light chains together under non-reducing conditions (Supplemental Figure 1). Additionally, the first amino acid of the mature MHC was mutated from a glycine to an alanine to improve sortase labeling efficiency. The murine IgG2a Fc was chosen as a backbone for the synTac heavy chain construct for its strong affinity for protein A-based purification methods to ensure high synTac yields. The sequence of the murine IgG2a Fc contains the well-characterized mutations L235A, E318A, K320A, and K322A to reduce antibody-dependent cellular cytotoxicity and complement-dependent cytotoxicity of the synTacs.[16, 17, 40]

SynTac Ag epitope cloning

For epitope cloning, the light chain vector was originally designed as an empty vector with a spacer epitope flanked by Type IIS BsmBI restriction sites to facilitate scar-free cloning (GAGACGACCTGGTGCCGATGATATCATCGATGGTGGCGACCGTCGTCTC; BsmBI sites underlined). The empty light chain vector is BsmBI digested, electrophoresed on a 0.8% agarose gel, and then gel purified using a PCR clean up and gel purification kit

(Macherey Nagel). The epitope encoding sequences are designed as annealed primer pairs with overhangs complementary to the overhangs left by BsmBI digestion. The annealed primers for the coding sequences used for each epitope in this study are as follows (BsmBI overhangs underlined): HPV $E7_{49–57}$: GGCCAGAGCCCATTACAATATTGTAACCTTTGCGG; IAV_$NP_{366–374}$: GGCCGCGTCTAACGAAAATATGGAAACCATGGCGG; LCMV_P14 ($GP_{33–41}$): GGCCAAGGCCGTGTACAACTTCGCCACCATGGCGG. Ligation is performed using the Rapid DNA Ligation kit (Roche) and is carried out with a 5X molar ratio of annealed epitope to digested vector. The ligation mixture is incubated for 5 min at room temperature (RT), then transformed into Stellar Competent Cells (*E. coli* HST08; Clontech). Colonies are selected on LB agar plates with kanamycin. Individual colonies are picked, grown in 2XYT broth with kanamycin, sequenced, and DNA stocks are prepared from sequence-confirmed colonies.

SynTac expression

SynTacs are produced using the ExpiCHO expression system (ThermoFisher). For all synTacs used in these experiments, heavy and light chain plasmids are cotransfected into the ExpiCHO cells. The ratio of heavy:light chain was optimized for each individual synTac (each unique epitope) by 1 mL small scale ExpiCHO transfections at different ratios of heavy:light plasmids. Supernatants from transfections were collected and synTacs were pulled down using protein A agarose beads (Pierce), then separated using SDS-PAGE in both non-reducing and reducing conditions to confirm the correct molecular weight of the full assembly and individual chains, respectively. For each epitope used here, 4:1 heavy:light chain demonstrated strong synTac expression in small scales and was subsequently used for all large-scale synTac transfections. SynTac plasmids were transfected according to the Max Titer protocol for the ExpiCHO expression system (ThermoFisher), and supernatants were harvested on day 14.

SynTac purification and storage

The supernatants from synTac-transfected ExpiCHO cells were centrifuged at 500 G followed by a second spin at 2500 G to ensure removal of cells and debris. The supernatants were then filtered through a 0.22 μm PES low protein-binding filter and purified on the AKTA Xpress FPLC system (GE Healthcare Life Sciences). Filtered supernatants were then affinity purified on the MabSelect SuRe column (GE Healthcare Life Sciences) as follows. First, the column was washed with 2 column volumes (CV) of 0.5M NaOH to strip endotoxins from the column, followed by 2 CV of MilliQ water. The column was then equilibrated using 5 CV 1X PBS equilibration buffer. Following completion of supernatant binding, the column was washed with 10 CV wash buffer 1 (1X PBS, 1 M NaCl final), then 5 CV wash buffer 2 (20 mM HEPES, 10 mM NaCl, pH 7.5), and eluted with 10 CV of 100% elution buffer (50 mM glycine, pH 2.8). Eluted fractions were neutralized immediately upon fractionation with 1 M Tris pH 9.0 to minimize structural damage due to low pH. Following affinity purification, the eluted fractions were pooled, filtered through a 0.22 μm filter to remove large insoluble aggregates, then purified via size exchange chromatography (SEC) using a Highload 26/60 Superdex 200 prep grade column (GE Healthcare Life Sciences) on the AKTA Xpress to remove any insoluble aggregates. SEC was performed by first washing

the Superdex 200 column in 1 CV 0.5 M NaOH to remove endotoxins from the column, followed by 1 CV of MilliQ water. The column was then equilibrated in 1.2 CV running buffer (1X PBS, 0.5 M NaCl final). Fractions were collected, pooled, and concentrated to ~2 mg/mL as measured by A280 on the NanoDrop 2000 system (ThermoFisher). SynTacs were then stored at this working concentration at 4°C until sortase reactions were performed. Non-reducing and reducing SDS-PAGE were performed on the concentrated synTacs to confirm purity and correct molecular weight of the intact heterodimer and individual chains, respectively (Supplemental Figure 1).

SynTacs stocks are stored no longer than 2 months at 4°C at the working concentrations of 2 mg/mL. Stocks can be kept at −20°C in 1X PBS, 0.5M NaCl, 10% glycerol for several months. Upon thawing frozen stocks or immediately preceding an experiment with a stock kept at 4°C for at least 1 month, the stock will be purified again on the Superdex 200 SEC column using 1X PBS with 0.5M NaCl as the running buffer to remove any aggregates formed during storage. Non-reducing and reducing SDS-PAGE gels are also run following SEC to ensure no degradation products are present from the pooled fractions.

SynTac molecular mass determination and comparison

30 μL of either E7 synTac or mouse anti-human CD28 monoclonal antibody (BD Pharmingen) was run over a 5μm, 4.6×300mm SRT SEC-300 column (Sepax) with each sample proceeding directly into the miniDAWN Treos MALS detector (Wyatt) upon eluting from the column. Here, the E7 synTac used for PET/CT imaging was compared to a mouse anti-human CD28 Ab to assess the MWs of our synTac constructs with respect to a conventional antibody. The MALS analysis was run for 20 minutes of the 25-minute SEC run, and MW data was compiled and compared to expected MW estimates based on literature or computational assessment of our synTac vectors using ProtParam (ExPASy).

SynTac modifications with sortase

SynTac heavy chains were expressed with a sortase recognition motif and 6X His-tag (LPETG-HHHHHH) at their C-termini for PET functionalization and purification, respectively (Figure 1A). Sortase reactions on synTacs for PET experiments were performed in PBS plus 0.5 M NaCl (pH 7.5) for 2 h at 20–25°C at ~2 mg/mL synTac, 500 μM nucleophile (i.e., $(Gly)_3$-NOTA), and 10 μM sortase A. Residual nucleophile was removed via a PD-10 size-exclusion column (GE Healthcare). Identity of the final products was confirmed by SDS-PAGE (e.g., Figure 1C).To evaluate sortase labeling efficiency, experiments were performed in which synTacs were labeled with $(Gly)_3$-Lys-biotin, run on SDS-PAGE (160V for 1 h on a 4–12% gradient Bis-Tris gel), transferred to polyvinylidene fluoride (PVDF) membranes, and stained with streptavidin-horseradish peroxidase (SA-HRP). Membranes were imaged with a BioRad ChemiDoc Imaging Station after the addition of an HRP-reactive chemiluminescent substrate (Western Lightning Plus-ECL, PerkinElmer). The purified enzymatically biotinylated synTac was compared to a mono-biotinylated standard (green fluorescent protein (GFP) quantified via 488 nm absorbance) (Supplemental Figure 3). The bands were quantified by densitometry using BioRad Image Lab software.

SynTac stability assay

To approximate synTac stability in circulation, synTacs were fluorescently-labeled with GGK-tetramethylrhodamine (TMR) (custom synthesized from Genscript) via a sortase reaction for tracking throughout the serum stability assay. Briefly, 7.5 μM synTac was reacted with 2 μM sortase A and 1.7 mM GGK-TMR for 2.5 hours at RT in the dark. Labeled synTac was then purified by gel filtration (S200 16/60, GE Life Sciences) and concentrated to 2 mg/mL. 60 μg of TMR-conjugated synTac was incubated in C57BL/6 serum (501003574, Innovative Research Inc.) at 37°C for the desired time, then the mixture was loaded into a 100 μL loop and run on an analytical gel filtration column (Superose 6 Increase 10/300 GL, GE Life Sciences). The column was run with 1X PBS, and 500 μL fractions were collected for the duration of the run. After each run had finished, 100 μL of each fraction was transferred to a clear-bottom 96-well assay plate (3904, Corning) and analyzed for TMR fluorescence (552 nm excitation, 580 nm emission) on an EnVision plate reader (2105–010, Perkin Elmer). Fluorescence reads were compiled and analyzed in GraphPad Prism. Each gel filtration run was compared to the fluorescence peaks from each well in the elution plate to determine if the synTac was aggregating, which would be evident in a shift of fluorescence toward the earlier void fractions, and no such shifts were observed at any time point up to 24 h (Supplemental Figure 4). This suggests that the synTacs would be stable in circulation for at least 24 h.

ELISpot assay

IFNγ ELISpot assays were performed as described.[41] Briefly, 96-well ELISpot plates (BD ELISPOT Mouse IFNγ ELISPOT Set, BD Biosciences, San Jose, CA) were coated with an IFNγ capture antibody (BD Biosciences) in PBS overnight (ON) at 4°C, and then plates were blocked with complete medium for 2 h at RT. Peptide or a synTac of known specificity (HPV E7 or IAV NP) was then added to wells, followed by the addition of 2.5×10^5 splenocytes (whole splenocytes to detect antigen-specific CD8 T cells is standard for optimized ELISpot assays),[42] 2×10^4 tumor cells, or 2×10^4 lung cells depending on the experiment. Positive control wells for all experiments contained 1X Cell Stimulation Cocktail (Invitrogen) prior to the addition of splenocytes or tumor cells, and negative control wells contained media only (Supplemental Figure 10). Plates were then washed and incubated with a biotinylated IFNγ detection antibody (BD Biosciences) for 2 h, followed by SA-HRP (BD Biosciences) for 1 h at RT. The plates were developed with 3-amino-9-ethyl-carbazole substrate (BD ELISPOT AEC Substrate Set) for 5 min and dried for at least 24 h. Spots were enumerated using the CTL ImmunoSpot S6 MACRO Analyzer.

HPV-induced cancer model

To study HPV-induced tumors, age-matched, 6-week-old female C57BL/6J mice were inoculated with 3×10^5 C3.43 cells. When tumors were palpable (~14 days later; see average tumor growth in Supplemental Figure 5), mice were treated intraperitoneally with VHH_{CD11b}-E7 plus adjuvant or adjuvant only. The adjuvant was 50 μg polyinosinic-polycytidylic acid (Poly(I:C) (Sigma Aldrich) and 50 μg anti-mouse CD40 (clone 1C10; Southern Biotech) as used previously.[22] For mice inoculated with both C3.43 and B16 cells, C3.43 cells were injected 6 days prior to inoculation with 1×10^5 B16 melanoma cells as B16

cells grow faster *in vivo*. Mice were treated with VHH_{CD11b}-E7 plus adjuvant or adjuvant only at ~14 days post C3.43 challenge (8 days post B16 challenge). Seven days later, mice were given the ^{64}Cu-labeled HPV E7 synTac by retroorbital injection and imaged by PET the following day (8 days post treatment). Following imaging, mice were euthanized and splenocytes and tumor cells were harvested, enumerated, and used for ELISpot analyses where indicated.

IAV acute infection model

IAV was quantified as described.[43] Age-matched, 6-week-old female C57BL/6J mice (3 per group) were anesthetized with isoflurane and infected intranasally with 40,000 infectious units of IAV WSN/33 diluted in PBS. Control mice were inoculated intranasally with an equal volume of PBS. Infection was tracked by monitoring daily weight loss. Eight days post infection, mice were given the ^{64}Cu-labeled IAV NP synTac by retroorbital injection and imaged by PET the following day (9 days post infection). After PET imaging, mice were euthanized; splenocytes and lung cells were harvested, enumerated and used for ELISpot assays where indicated.

ImmunoPET imaging of bulk CD8 T cells with an anti-CD8 VHH imaging agent

Radiolabeling of the anti-CD8 VHH with ^{89}Zr (VHH_{CD8}-^{89}Zr) was performed as described.[3] Briefly, VHH_{CD8} was conjugated to G_3-desferrioxamine (DFO)-azide via $SrtA_{staph7M}$. The azide group was used to install 20 kDa polyethylene glycol (PEG) moiety conjugated to dibenzocyclooctyne (as DBCO-PEG), which improves the quality of the PET signal seen with the anti-CD8 VHH *in vivo*.[3] A volume of ^{89}Zr stock solution (1.0 M oxalic acid adjusted to pH 6.8–7.5 using 2.0 M Na_2CO_3) corresponding to 1.0−1.5 mCi was added to 200 μL VHH_{CD8}-DFO solution (~2.0 mg of chelexed PEGylated-VHH_{CD8}-DFO in 0.5 M HEPES buffer, pH 7.5) in a 2 mL microcentrifuge tube, and the total volume was adjusted to 300 μL using 1.0 M oxalic acid. The reaction mixture was incubated for 60 min at RT with agitation, loaded onto a PD-10 size-exclusion column (GE Healthcare), and eluted with PBS. PET-CT was performed following published procedures.[21] Briefly, mice were anaesthetized using isoflurane, injected with ~25 μCi (925 kBq) radiolabeled VHH via by retroorbital injection, and imaged by PET-CT 24 h later using a G8 PET-CT small animal scanner (PerkinElmer, Norwalk, CT). PET and CT acquisition was ~10 min and 1.5 min, respectively, per animal. Images were reconstructed using the manufacturer's software. Specifically, scans of 20 million counts per mouse were obtained using a PET/CT scanner (Perkin Elmer) and reconstructed using the 3D ordered subsets expectation maximization protocol.

ImmunoPET imaging and analysis with synTacs

Chelation of radiometals to the NOTA-labeled synTacs was performed as described.[3] We have compared different radioisotopes in the context of the synTac imaging agent and found that the use of ^{64}Cu yields images of excellent quality. Use of the NOTA chelator for installation of ^{64}Cu is straightforward and more convenient than the use of ^{18}F. The use of ^{89}Zr is complicated by the need to rigorously remove contaminating metal ions that can be complexed by DFO. This is done through chelexing, with an attendant, unacceptable loss of the synTac in the course of this process. We did not observe such losses for the much smaller

^{89}Zr-PEG$_{20}$-anti-CD8 VHH imaging agent. The circulatory half-life of the synTacs (~12 min; Supplemental Figure 6) is also much shorter than that of full-sized antibodies, thus a longer radioactive half-life is not necessary, and isotopes with shorter half-lives may be preferable to minimize radiation exposure if translated to the clinic. Thus, sortase-ready synTacs were labeled with $^{64}CuCl_2$ (4 mCi in 10 μL 200 mM NH_4OAc solution; pH 6.5 followed by dilution into 100 uL PBS) following chelation to G_3-NOTA installed via $SrtA_{staph7M}$. ^{64}Cu was purchased from the Washington University School of Medicine MIR Cyclotron Facility with radionuclide purity of >95% for all experiments with effective specific activities of ~500–1200 mCi/μg as measured by the supplier. The reaction mixture was incubated for 20 min at RT with agitation and loaded onto a PD-10 size-exclusion column (GE Healthcare). Elution with PBS yielded the imaging agent separated from free label. The specific activity of the ^{64}Cu-labeled synTacs was ~2 μCi/μg, and the purity of the labeled synTacs was shown to be >95% by thin-layer chromatography (TLC; Supplemental Figure 11).

PET-computed tomography (PET-CT) was performed following published procedures.[21] Briefly, mice (C3.43 tumor-bearing, IAV-infected, FcRn KO, or control mice) were anaesthetized using isoflurane, injected with ~50 μCi (1850 kBq) of ^{64}Cu-labeled synTac (~25 μg total protein) by retroorbital injection, and imaged by PET-CT 24 h later (~10 μCi/mouse), using a G8 PET-CT small-animal scanner (PerkinElmer, Norwalk, CT). PET and CT acquisition time was ~10 min and 1.5 min, respectively, per animal. The image quality is a function of both the dose and time of the scan. We have seen that a 10 min scan at the indicated dose yields images of the desired quality (Supplemental Figure 12). Images were reconstructed using the manufacturer's software. PET images were scaled based on the highest and lowest intensities and were set at 1.5–15 %ID/g for all images obtained with ^{64}Cu-labeled synTacs 24 h after injection unless otherwise noted. CT contrast was set to −600–3000 Hounsfield units/mm3 (HU) for all images. Data were further analyzed and quantified using VivoQuant software (inviCRO Imaging Service and Software, Boston, MA).

PET values were quantified in 3D regions of interest (ROIs) using the CT scans as a reference. For ectopic tumors, ROIs were drawn manually (unblinded) from masses observed in the CT image (Supplemental Figure 13A–B). For the lungs, ROIs were created for each image corresponding to preset CT values (−600 to 0 HU) in the ribcage, surrounding the heart as a means of identifying pulmonary space (Supplemental Figure 13C–D). An additional ROI was drawn in the muscle tissue of the hindleg of each mouse, avoiding bones. Once all ROIs were generated, statistical information for each ROI containing mean PET signals as %ID/g was exported as a table and processed (Sup. Tables 1–4). We normalized %ID/g values from tumors and lungs to background values observed in hindleg muscle tissue for each mouse.

In separate experiments, synTacs were labeled with ^{89}Zr (chelated with GGG-DFO) and ^{18}FDG (tetrazine-labeled for attachment to a synTac functionalized with *trans*-cyclooctene (TCO) via sortase) using methods established in the laboratory.[3,23] Though ^{64}Cu was used for the majority of synTac imaging for reasons explained above, ^{89}Zr and ^{18}FDG were included to determine if they or their associated attachment molecules would effect liver

uptake. Mice were anaesthetized using isoflurane, injected with ~60 μCi (2220 kBq) ^{18}F-labeled or ~30 μCi (1110 kBq) ^{89}Zr-labeled synTac (~25 μg total protein) by retroorbital injection, and imaged by PET-CT 24 h later, using a G8 PET-CT small-animal scanner (PerkinElmer, Norwalk, CT). PET and CT acquisition time was ~10 min and 1.5 min, respectively, per animal. Images were reconstructed using the manufacturer's software. The injected doses (~60 μCi for ^{18}F and ~30 μCi for ^{89}Zr) were such that all mice had ~10 μCi total radioactivity at the time of scanning (4 h post injection for ^{18}F and 24 h for ^{89}Zr). The loss in radioactivity at the time of scanning compared to the injected dose is a combination of clearance via secretion in urine and radioactive half-life of the isotope. Thus, the^{18}F and ^{89}Zr images were obtained with radioactivities comparable to those obtained with ^{64}Cu and were obtained well beyond the measured circulatory half-life of the synTacs as noted above.

Synthesis of $(Gly)_3$-NOTA-azide

The peptide $(Gly)_3$-PEG_3-Cys-PEG_3-Lys(azide) with amidation at the C-terminus (see structure in Supplemental Figure 14A) was synthesized by standard solid-phase peptide synthesis and was dissolved in 50 mM $NaHCO_3$ buffer, pH 8.3. Maleimide-NOTA (from Macrocyclics) was dissolved in DMSO. The peptide was added to the maleimide-NOTA solution and mixed at RT for 1 h until LC-MS analysis indicated near-complete conversion to the product. The solution was filtered and purified by reverse phase-HPLC with a semi-preparative column (C18 column, Gemini, 5 μm, 10 × 250 mm; Phenomenex) at a flow rate of 4.5 mL/min; solvent A: 0.1% TFA in H_2O, solvent B: 0.1% TFA in CH_3CN. $(Gly)_3$-PEG_3-Cys(NOTA)-PEG_3-Lys(azide) eluted at 50–55% solvent B. Fractions containing pure product were collected and lyophilized. LC-MS, calculated at 1,277.61 for $C_{51}H_{88}N_{16}O_{20}S$ $[M+H]^+$, found an observed mass at 1277.00 (Supplemental Figure 14B).

PEGylation of synTacs

The HPV E7 synTac was conjugated to $(Gly)_3$-NOTA-azide via $SrtA_{staph7M}$ as described above for G_3-NOTA. The azide group was used to install a 20 kDa PEG moiety (as DBCO-PEG) as described.[3] The un-PEGylated and PEGylated synTacs (both labeled with NOTA) were separated via SDS-PAGE (160V for 1 h on a 4–12% gradient Bis-Tris gel), and the gels were stained with a Coomassie blue dye (InstantBlue, Expedeon, Cambridgeshire, UK). The gels were then imaged with a BioRad ChemiDoc Imaging Station and the bands were quantified using BioRad Image Lab. PEGylation efficiency was calculated as density PEGylated band/(PEGylated band + un-PEGyled band) from the same lane (Figure 6A) and was found to be ~90%. The NOTA-labeled synTacs with and without PEG were chelated with ^{64}Cu, and ~50 μCi (1850 kBq) of ^{64}Cu-labeled synTacs (~25 μg total protein) were injected by retroorbital injection for PET imaging of mice harboring C3.43 tumors treated with VHH_{CD11b}-E7 plus adjuvant-treated as described above.

PNGase Digestion of SynTacs

IAV NP synTacs were treated with peptide:N-glycosidase F (PNGase F; NEB Biosciences) to remove N-linked glycans from the Fc portion following the manufacturer's protocol prior to conjugation with $(Gly)_3$-NOTA for PET imaging. Briefly, synTacs (2 mg/mL) were incubated with PNGase F (10 μg synTac: 1 uL PNGase F as suggested by manufacturer) at 37°C ON. Mock digestion (no PNGase, 37°C ON incubation) was used as a control.

PNGase F-digested and undigested synTacs synTacs were separated via SDS-PAGE (160V for 1 h on a 4–12% gradient Bis-Tris gel), and the gels were stained with a Coomassie blue dye (InstantBlue, Expedeon, Cambridgeshire, UK). The gels were then imaged with a BioRad ChemiDoc Imaging Station and the bands were quantified using BioRad Image Lab. Removal of the glycans by PNGase F digestion resulted in a reduction in apparent molecular (Figure 6D). PNGase F-digested and undigested synTacs were then conjugated to $(Gly)_3$-NOTA via $SrtA_{staph7M}$ and labeled with ^{64}Cu as described above. PNGase F-digested and undigested ^{64}Cu-labeled IAV NP synTacs were injected by retroorbital injection (~50 μCi (1850 kBq)/mouse) for PET imaging of IAV-infected mice as described above.

Statistical analyses

Statistical analyses were performed on GraphPad Prism version 7.0 (GraphPad Software Inc., San Diego, CA). Statistical significance for differences in PET signal intensity was assessed with two-tailed unpaired Student's *t* tests. Significance was defined as $p < 0.05$ for all experiments.

Data availability

The data that support the findings of this study are available from the corresponding author upon reasonable request.

Supplementary Material

Refer to Web version on PubMed Central for supplementary material.

Acknowledgments

AWW is supported by the Arnold O. Beckman Postdoctoral Fellowship. RWC is supported in part by funding from the Cancer Research Institute Irvington Postdoctoral Fellowship. MR is an American Cancer Society Fellow. HLP is supported by the Lustgarten Foundation (award ID 388167). The authors would also like to acknowledge VIR Biotechnology and Cue Biopharma for partial support of this work. The synTac technology was developed with support provided by the NIH (U01GM094665, U54GM094662, R01AI145024 and R01CA198095 to SCA). We acknowledge the Wollowick Family Foundation Chair in Multiple Sclerosis and Immunology (to SCA), and Janet & Martin Spatz and the Helen & Irving Spatz Foundation. Additional support provided by the Albert Einstein Macromolecular Therapeutics Development Facility, the Einstein-Rockefeller-CUNY Center for AIDS Research (P30AI124414), and the Albert Einstein Cancer Center (P30CA013330).

References

1. Rashidian M et al. Predicting the response to CTLA-4 blockade by longitudinal noninvasive monitoring of CD8 T cells. J Exp Med 214, 2243–2255 (2017). [PubMed: 28666979]
2. Wu AM Antibodies and antimatter: the resurgence of immuno-PET. J Nucl Med 50, 2–5 (2009). [PubMed: 19091888]
3. Tavare R et al. An Effective Immuno-PET Imaging Method to Monitor CD8-Dependent Responses to Immunotherapy. Cancer Res 76, 73–82 (2016). [PubMed: 26573799]
4. Dey S et al. Tracking antigen specific T-cells: Technological advancement and limitations. Biotechnol Adv 37, 145–153 (2019). [PubMed: 30508573]
5. Alam IS et al. Imaging activated T cells predicts response to cancer vaccines. J Clin Invest 128, 2569–2580 (2018). [PubMed: 29596062]
6. Larimer BM et al. Granzyme B PET Imaging as a Predictive Biomarker of Immunotherapy Response. Cancer Res 77, 2318–2327 (2017). [PubMed: 28461564]

7. Gibson HM et al. IFNgamma PET Imaging as a Predictive Tool for Monitoring Response to Tumor Immunotherapy. Cancer Res 78, 5706–5717 (2018). [PubMed: 30115693]
8. Marciscano AE & Thorek DLJ Role of noninvasive molecular imaging in determining response. Adv Radiat Oncol 3, 534–547 (2018). [PubMed: 30370353]
9. Vyas JM, Van der Veen AG & Ploegh HL The known unknowns of antigen processing and presentation. Nat Rev Immunol 8, 607–618 (2008). [PubMed: 18641646]
10. Skeate JG, Woodham AW, Einstein MH, Da Silva DM & Kast WM Current therapeutic vaccination and immunotherapy strategies for HPV-related diseases. Hum Vaccin Immunother 12, 1418–1429 (2016). [PubMed: 26835746]
11. Sebzda E et al. Selection of the T cell repertoire. Annu Rev Immunol 17, 829–874 (1999). [PubMed: 10358775]
12. Davis MM et al. Ligand recognition by alpha beta T cell receptors. Annu Rev Immunol 16, 523–544 (1998). [PubMed: 9597140]
13. Huppa JB & Davis MM T-cell-antigen recognition and the immunological synapse. Nat Rev Immunol 3, 973–983 (2003). [PubMed: 14647479]
14. Doherty PC The tetramer transformation. J Immunol 187, 5–6 (2011). [PubMed: 21690330]
15. Altman JD et al. Phenotypic analysis of antigen-specific T lymphocytes. Science 274, 94–96 (1996). [PubMed: 8810254]
16. Duncan AR & Winter G The binding site for C1q on IgG. Nature 332, 738–740 (1988). [PubMed: 3258649]
17. Wines BD, Powell MS, Parren PW, Barnes N & Hogarth PM The IgG Fc contains distinct Fc receptor (FcR) binding sites: the leukocyte receptors Fc gamma RI and Fc gamma RIIa bind to a region in the Fc distinct from that recognized by neonatal FcR and protein A. J Immunol 164, 5313–5318 (2000). [PubMed: 10799893]
18. Feltkamp MC et al. Vaccination with cytotoxic T lymphocyte epitope-containing peptide protects against a tumor induced by human papillomavirus type 16-transformed cells. Eur J Immunol 23, 2242–2249 (1993). [PubMed: 7690326]
19. Rotzschke O et al. Isolation and analysis of naturally processed viral peptides as recognized by cytotoxic T cells. Nature 348, 252–254 (1990). [PubMed: 1700304]
20. Gallimore A et al. A protective cytotoxic T cell response to a subdominant epitope is influenced by the stability of the MHC class I/peptide complex and the overall spectrum of viral peptides generated within infected cells. Eur J Immunol 28, 3301–3311 (1998). [PubMed: 9808199]
21. Rashidian M et al. Noninvasive imaging of immune responses. Proc Natl Acad Sci U S A 112, 6146–6151 (2015). [PubMed: 25902531]
22. Woodham AW et al. Nanobody-Antigen Conjugates Elicit HPV-Specific Antitumor Immune Responses. Cancer Immunol Res 6, 870–880 (2018). [PubMed: 29792298]
23. Rashidian M et al. The use of (18)F-2-fluorodeoxyglucose (FDG) to label antibody fragments for immuno-PET of pancreatic cancer. ACS Cent Sci 1, 142–147 (2015). [PubMed: 26955657]
24. Walboomers JM et al. Human papillomavirus is a necessary cause of invasive cervical cancer worldwide. J.Pathol. 189, 12–19 (1999). [PubMed: 10451482]
25. Stanley MA, Pett MR & Coleman N HPV: from infection to cancer. Biochem Soc Trans 35, 1456–1460 (2007). [PubMed: 18031245]
26. Feltkamp MC et al. Cytotoxic T lymphocytes raised against a subdominant epitope offered as a synthetic peptide eradicate human papillomavirus type 16-induced tumors. Eur J Immunol 25, 2638–2642 (1995). [PubMed: 7589138]
27. Kanodia S et al. Expression of LIGHT/TNFSF14 combined with vaccination against human papillomavirus Type 16 E7 induces significant tumor regression. Cancer Research 70, 3955–3964 (2010). [PubMed: 20460520]
28. Thomas PG, Keating R, Hulse-Post DJ & Doherty PC Cell-mediated protection in influenza infection. Emerg Infect Dis 12, 48–54 (2006). [PubMed: 16494717]
29. Wu AM Engineered antibodies for molecular imaging of cancer. Methods 65, 139–147 (2014). [PubMed: 24091005]

30. Sheeley DM, Merrill BM & Taylor LC Characterization of monoclonal antibody glycosylation: comparison of expression systems and identification of terminal alpha-linked galactose. Anal Biochem 247, 102–110 (1997). [PubMed: 9126378]
31. Roggenbuck D, Mytilinaiou MG, Lapin SV, Reinhold D & Conrad K Asialoglycoprotein receptor (ASGPR): a peculiar target of liver-specific autoimmunity. Auto Immun Highlights 3, 119–125 (2012). [PubMed: 26000135]
32. Pyzik M et al. Hepatic FcRn regulates albumin homeostasis and susceptibility to liver injury. Proc Natl Acad Sci U S A 114, E2862–E2871 (2017). [PubMed: 28330995]
33. Sockolosky JT & Szoka FC The neonatal Fc receptor, FcRn, as a target for drug delivery and therapy. Adv Drug Deliv Rev 91, 109–124 (2015). [PubMed: 25703189]
34. Weissleder R, Schwaiger MC, Gambhir SS & Hricak H Imaging approaches to optimize molecular therapies. Sci Transl Med 8, 355ps316 (2016).
35. Mall S et al. Immuno-PET Imaging of Engineered Human T Cells in Tumors. Cancer Res 76, 4113–4123 (2016). [PubMed: 27354381]
36. Seo JW et al. CD8(+) T-Cell Density Imaging with (64)Cu-Labeled Cys-Diabody Informs Immunotherapy Protocols. Clin Cancer Res 24, 4976–4987 (2018). [PubMed: 29967252]
37. Pyzik M et al. The neonatal Fc Receptor (FcRn): A misnomer? Front. Immunol 10, (2019).
38. Quayle SN et al. CUE-101, a Novel HPV16 E7-pHLA-IL-2-Fc Fusion Protein, Enhances Tumor Antigen Specific T Cell Activation for the Treatment of HPV16-Driven Malignancies. Clin. Cancer Res. clincanres.3354.2019 (2020).
39. Guimaraes CP et al. Site-specific C-terminal and internal loop labeling of proteins using sortase-mediated reactions. Nat Protoc 8, 1787–1799 (2013). [PubMed: 23989673]
40. Steurer W et al. Ex vivo coating of islet cell allografts with murine CTLA4/Fc promotes graft tolerance. J Immunol 155, 1165–1174 (1995). [PubMed: 7543517]
41. Yan L, Woodham AW, Da Silva DM & Kast WM Functional analysis of HPV-like particle-activated Langerhans cells in vitro. Methods Mol Biol 1249, 333–350 (2015). [PubMed: 25348318]
42. Carvalho LH, Hafalla JC & Zavala F ELISPOT assay to measure antigen-specific murine CD8(+) T cell responses. Journal of immunological methods 252, 207–218 (2001). [PubMed: 11334981]
43. Schmidt FI et al. Phenotypic lentivirus screens to identify functional single domain antibodies. Nat Microbiol 1, 16080 (2016). [PubMed: 27573105]

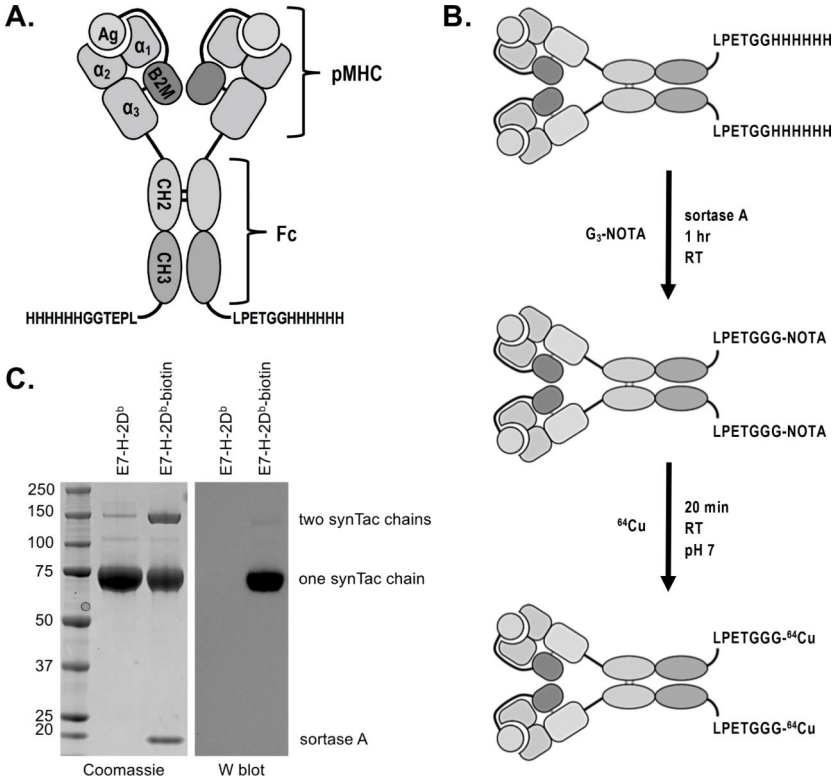

Figure 1.

SynTac design, validation, and labeling strategy. A) Two pMHC (H-2D^b) molecules are covalently attached to an IgG2a Fc region. The antigen is expressed as a fusion with B2M. A 6X His-tag and sortase recognition motif (LPETG) have been installed at the C-terminus of each CH3 domain for purification and site-specific protein modification via sortase, respectively. B) Schematic of ^{64}Cu-labeled synTac preparation for immunoPET imaging. Sortase was used to install the metal chelator G_3-NOTA (NOTA: 1,4,7-triazacyclononane-N,N',N"-triacetic acid), which is then radiolabeled with ^{64}Cu prior to imaging. C) Coomassie stain (left) and western blot (right) of the HPV E7 H-2D^b synTac before and after conjugation with G_3-biotin via sortase. The samples were separated via SDS-PAGE under reducing conditions and stained with Coomassie reagent (left) or transferred to a PVDF membrane and probed with streptavidin-HRP (right). The synTac heavy chain runs at ~75 kDa when the disulfide bonds between the CH2 domains are reduced. The western blot shows that biotin was successfully installed on the synTac as only the sortase-modified sample results in luminescence when incubated with streptavidin-HRP and an HRP substrate. Shown is a representative example of an experiment performed three times.

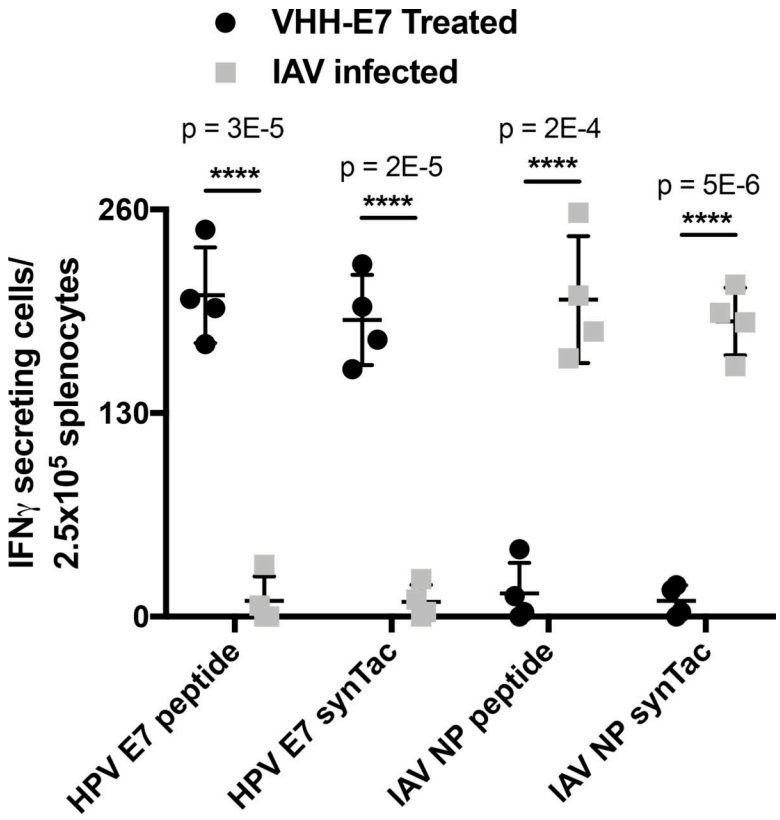

Figure 2.

Analysis of synTac specificity *in vitro*. Splenocytes from C57BL/6 mice treated with VHH_{CD11b}-E7 (shortened as VHH-E7) plus adjuvant or from IAV-infected mice were incubated overnight with HPV $E7_{49–57}$ (RAHYNIVTF), HPV E7 synTac, IAV $NP_{366–374}$ (ASNENMETM), or IAV NP synTac (100 nM equivalent). The number of IFN-γ-secreting cells was measured via ELISpot assay. Shown are means ± SD of an experiment performed in quadruplicate (biological replicates and is representative of two independent experiments (****$p < 0.0001$; two-sided Student's t-test).

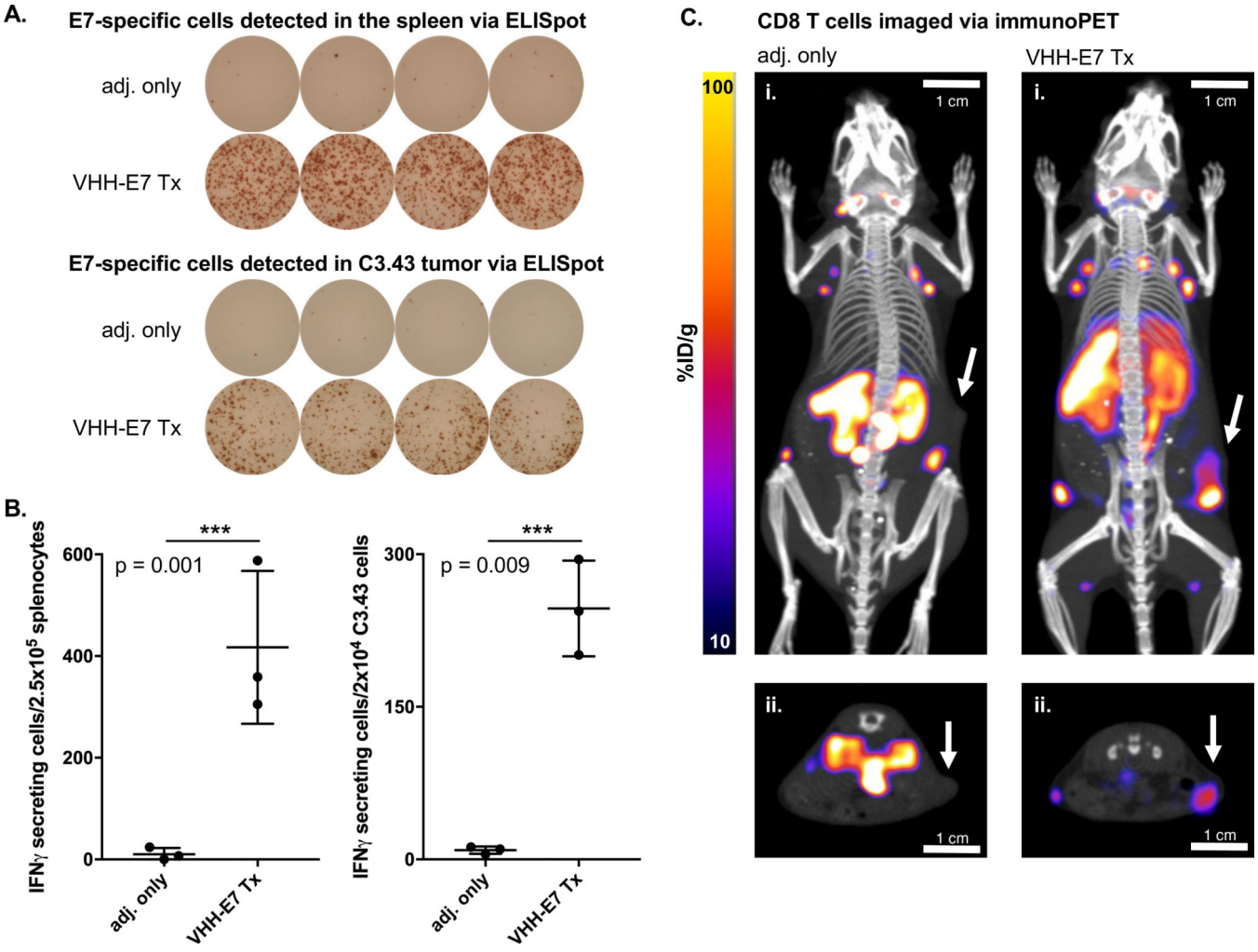

Figure 3.

ELISpot analysis of HPV E7-specific T cells in (shortened as VHH-E7 above) treated mice and detection of CD8 T cells in HPV E7-expressing tumors by VHH-based immunoPET. Wild-type C57BL/6 mice were challenged with 3×10^5 C3.43 cells. When tumors were palpable (~14 days later), mice were treated IP with adjuvant (adj. = 50 μg Poly(I:C) + 50 μg agonistic anti-CD40 Ab) or VHH_{CD11b}-E7 plus adjuvant (n = 3/group). 8 days after treatment, spleens and tumors were harvested and $E7_{49–57}$-specific CD8 T cells were enumerated via IFN-γ ELISpot. A) Representative examples of quadruplicate wells of the ELISpot assay. B) Quantification of IFN-γ secreting cells detected in the spleens (left) and C3.43 tumors (right) of the treated mice (means ± SD are shown; n = 3; ***$p < 0.001$; two-sided Student's t-test). C) C3.43 tumor-bearing mice from (B) were retro-orbitally injected with an anti-CD8 VHH labeled with ^{89}Zr 7 days after treatment and imaged the following day by PET-CT prior to spleen and tumor resection. Representative PET-CT images are shown. White arrows in the maximal intensity projection (MIP) coronal (i) and transverse (ii) images indicate the sites of the tumors.

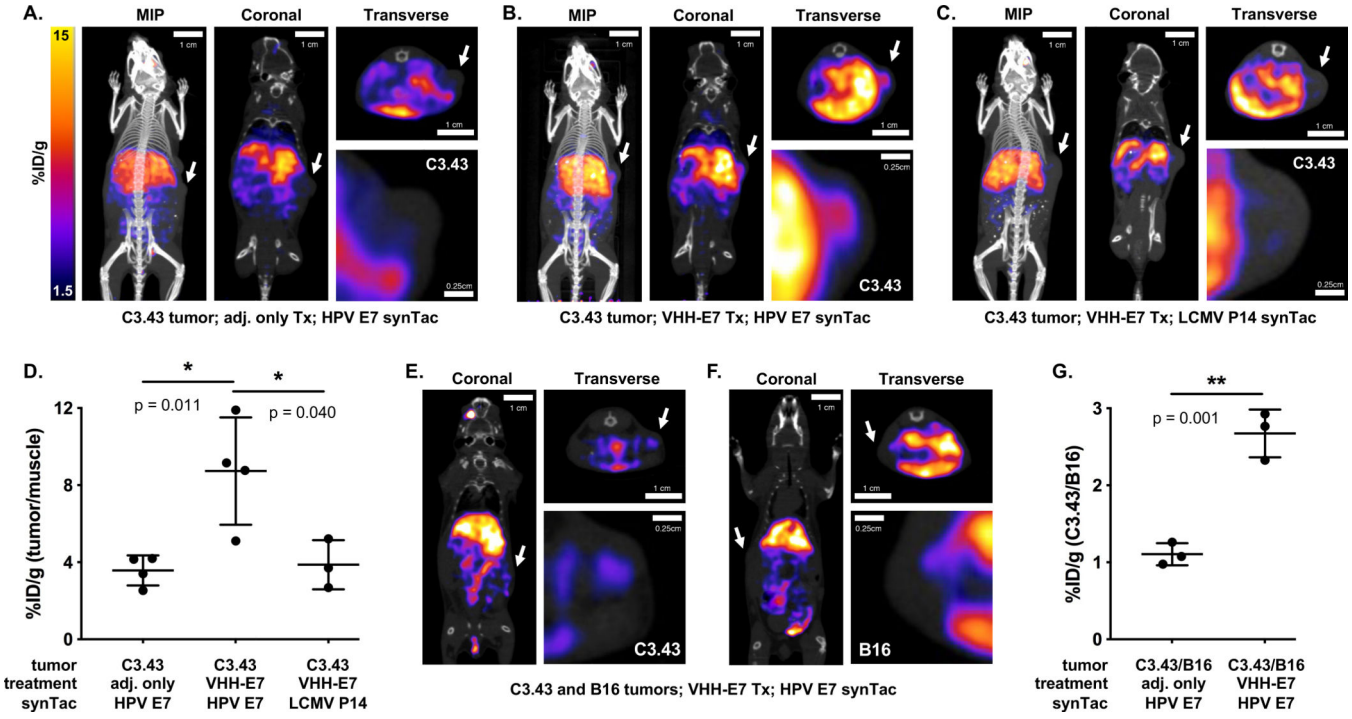

Figure 4.

PET-CT imaging with the HPV E7 synTac. A-C) C3.43 tumor-bearing C57BL/6 mice were either treated with adjuvant only (A) or VHH_{CD11b}-E7 (shortened as VHH-E7) plus adjuvant (B-C). ~50 μCi (1850 kBq) ^{64}Cu-labeled HPV E7 (A-B) or LCMV P14 (C) synTac was injected retro-orbitally 7 days after treatment, and PET-CT scanning was performed the next day (8 days after treatment). Representative MIP, coronal, and transverse (cross-section of tumor) PET-CT images are shown with close-up images of the transverse tumor sections in which PET signal is only seen in the tumors of VHH_{CD11b}-E7 treated mice imaged with the ^{64}Cu-labeled HPV E7 synTac (B). White arrows indicate the location of the tumors. D) Quantification of C3.43 intratumoral PET signals over background signal (hindleg muscle) as observed in mice from (A-C) (means ± SD are shown; n = 4/group; *$p < 0.05$; two-sided Student's t-test). E-F) C3.43 and B16 co-tumor-bearing mice were treated with VHH_{CD11b}-E7 plus adjuvant. ^{64}Cu-labeled HPV E7 synTac was injected 7 days after treatment, and PET-CT scanning was performed the next day (8 days after treatment). Representative coronal and transverse PET-CT images are shown with close-up images of the tumors. A C3.43 (E; white arrows) and B16 tumor (F; white arrows) are shown separately from the same mouse. PET signal was greater in C3.43 tumors that expressed the appropriate HPV E7 antigen than that of B16 tumors in the same animal. G) Quantification of PET signals observed in C3.43 tumors over those observed in B16 tumors of mice treated with adjuvant only or VHH_{CD11b}-E7 plus adjuvant (means ± SD are shown; n = 4/group; **$p < 0.05$; two-sided Student's t-test).

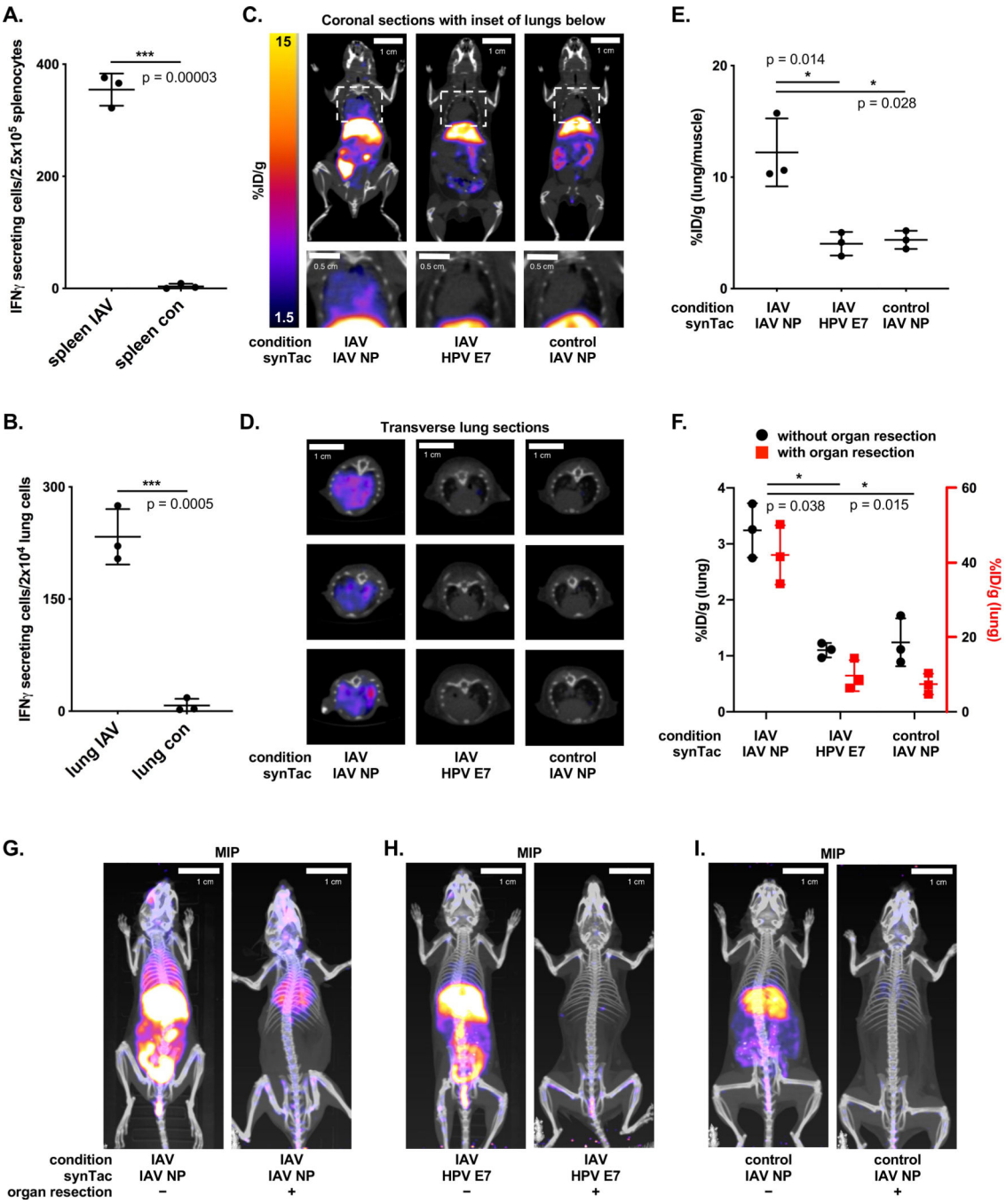

Figure 5.

PET-CT imaging with the IAV NP synTac. Non-tumor bearing C57BL/6 mice were infected with IAV via nasal drip 9 days prior to analysis of IAV NP-specific CD8 T cells. A-B) ELISpot analysis of IAV NP-specific CD8 T cell responses in the spleens (A) and lungs (B) of IAV-infected or uninfected control mice (means ± SD are shown; n = 3/group; ***p < 0.001; two-sided Student's t-test). C-D) Coronal (C; full body top and close-up of lungs bottom) and transverse (D) PET-CT images of IAV-infected mice retro-orbitally injected with ^{64}Cu-labeled IAV NP synTac (left) or ^{64}Cu-labeled HPV E7 synTac (middle) 9 days

after IAV infection. Uninfected control mice were imaged with the ^{64}Cu-labeled IAV NP synTac (right). E) Quantification of ^{64}Cu-labeled IAV NP synTac PET signal in the lungs of IAV-infected or control mice over background signal (hindleg muscle). Mice were injected with ^{64}Cu-labeled IAV NP synTac 8 days after IAV infection and PET-CT scanning was performed the next day (9 days after infection). IAV-infected mice were also given the ^{64}Cu-labeled HPV E7 synTac in which the PET signal in the lungs was similar to that observed in uninfected mice (means ± SD are shown; n = 3/group; *p <0.05). F) Quantification of synTac PET signals in the lungs before (black) and after (red) abdominal organ resection. The function of the red axis (right) is to show the value of the signal in the lungs after organ resection and coordinates with the red points in the graph. IAV-infected mice were injected with ^{64}Cu-labeled IAV NP or HPV E7 synTac 8 days after IAV infection and PET-CT imaging was performed the next day (9 days after infection). Uninfected control mice were given the ^{64}Cu-labeled IAV NP synTac (means ± SD are shown; n = 3/group; *p <0.05). G-I) PET-CT imaging with synTacs before (left) and after (right) abdominal organ resection. IAV-infected mice were injected with ^{64}Cu-labeled IAV NP synTac (G) or ^{64}Cu-labeled HPV E7 synTac (H) 8 days after IAV infection and PET-CT imaging was performed the next day (9 days after infection). I) Uninfected control mice were imaged with the ^{64}Cu-labeled IAV NP synTac. Shown are representative MIP PET-CT images of the same mice before (left) and after (right) abdominal organ resection (n = 3/group).

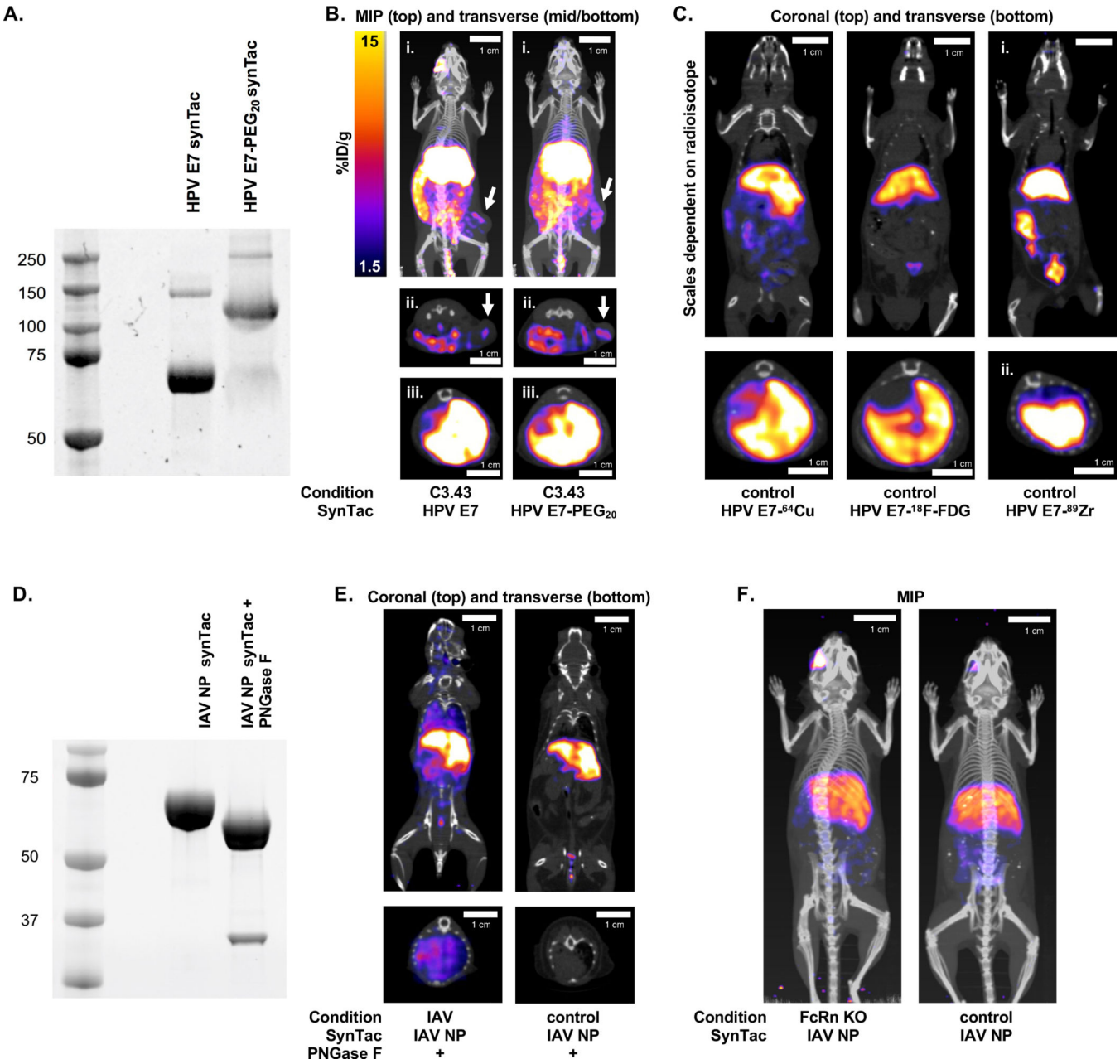

Figure 6.

SynTac PET-CT imaging following different radio-labeling strategies. A) G_3-NOTA-azide was attached to the HPV E7 synTac via sortase followed by the addition of a 20 kDa PEG (PEG_{20}) moiety (as DBCO-PEG_{20}) with a click reaction. PEGylation of the synTac was verified as an upward size-shift (~40 kDa as two PEG_{20} moieties are attached per synTac; i.e., one per chain) following PAGE and Coomassie staining (right lane). B) C3.43 tumor-bearing mice were treated with VHH_{CD11b}-E7 plus adjuvant. Mice were then retro-orbitally injected with ^{64}Cu-labeled HPV E7 synTac (left) or PEGylated ^{64}Cu-labeled HPV E7 synTac (right) 7 days after treatment, and PET-CT scanning was performed the next day (8 days after treatment). Representative MIP (i. whole body) and transverse (ii. cross-section of

tumors; iii. cross-section of livers) PET-CT images are shown. C) PET-CT scanning was performed on wild-type C57BL/6 mice injected with HPV E7 synTac labeled with ^{64}Cu (imaged the following day), ^{18}F-FDG (imaged 4 hrs after injection), or ^{89}Zr (imaged the following day). Scaling for ^{64}Cu and ^{18}F-FDG are the same as in B and the ^{89}Zr image is scaled at 1.5–30 %ID/g. Representative coronal (top; whole body) and transverse (bottom; cross-section of livers) PET-CT images are shown. D) The IAV NP synTac was pre-treated with PNGase F resulting in deglycosylation of the Fc region as observed by a downward size-shift following SDS-PAGE and Coomassie staining (right lane). The bottom band in the right lane is PNGase F (~36 kDa). E) Mice were injected with PNGase F-digested ^{64}Cu-labeled IAV NP synTac 8 days after IAV infection and PET-CT imaging was performed the next day (9 days after infection) (left). Uninfected control mice were also imaged with the PNGase F-digested ^{64}Cu-labeled IAV NP synTac (right). Shown are representative coronal (top) and transverse (bottom; cross-section of lungs) PET-CT images of an IAV-infected and uninfected mouse. F) FcRn knock-out (KO) and wild-type C57BL/6 mice were injected with ^{64}Cu-labeled IAV NP synTac and PET-CT imaging was performed the next day. Representative MIP PET-CT images are shown. All experiments shown were performed at least three independent times with similar results.